ENGINEERING

Tunable electroresistance and electro-optic effects of transparent molecular ferroelectrics

Zhuolei Zhang,[1] Peng-Fei Li,[2] Yuan-Yuan Tang,[2] Andrew J. Wilson,[3] Katherine Willets,[3] Manfred Wuttig,[4]* Ren-Gen Xiong,[2]* Shenqiang Ren[1]*

Recent progress in molecular ferroelectrics (MOFEs) has been overshadowed by the lack of high-quality thin films for device integration. We report a water-based air-processable technique to prepare large-area MOFE thin films, controlled by supersaturation growth at the liquid-air interface under a temperature gradient and external water partial pressure. We used this technique to fabricate $ImClO_4$ thin films and found a large, tunable room temperature electroresistance: a 20-fold resistance variation upon polarization switching. The as-grown films are transparent and consist of a bamboo-like structure of $(2,\bar{1},0)$ and $(1,0,\bar{2})$ structural variants of *R*3*m* symmetry with a reversible polarization of 6.7 μC/cm^2. The resulting ferroelectric domain structure leads to a reversible electromechanical response of d_{33} = 38.8 pm/V. Polarization switching results in a change of the refractive index, *n*, of single domains, $\frac{\Delta n}{n}$ = 0.3. The remarkable combination of these characteristics renders MOFEs a prime candidate material for new nanoelectronic devices. The information that we present in this work will open a new area of MOFE thin-film technologies.

INTRODUCTION

The first molecular ferroelectric (MOFE) crystal, Rochelle salt, was discovered in 1921 (*1*). The switchable polarization of MOFE crystals is useful in modern memory and capacitor elements (*2*–*8*), and their secondary characteristics, piezoelectricity, pyroelectricity, and electro-optic activity (*9*–*11*), have technological potential in actuators, sensors, and transducers (*12*–*14*). Whereas magnetoresistance is well known and serves as the basis of the reading mechanism of modern magnetic memories, electroresistance of MOFEs is much less known, let alone used in devices (*3*, *15*–*17*). However, a way of determining their controlled deposition on arbitrary supports in the form of thin films should be found, considering that both large-area solution processability and crystal flexibility are rare themselves, lagging behind of their inorganic oxide counterparts (*18*).

The low symmetry of MOFEs poses difficulties because each film grain crystallite can be polarized in only one direction determined at the time of thin-film formation, which is either random or unfavorably distributed in most cases (*19*, *20*). Hence, without appropriate control of the crystallite orientations, only a small portion of structural and electrical domains can be effectively switched. This inadequate orientation control of MOFEs has, so far, limited practical applications in molecular electronics, in drastic contrast to inorganic perovskites whose high-symmetry polarization can be electrically oriented by poling, which renders polycrystalline perovskite ceramics the most industrially valuable ferroelectric material (*21*, *22*). Here, we present the first report on the preparation of high-quality large-area MOFE films using in-plane liquid-phase (IP-LP) growth (Fig. 1). This generally applicable approach allows precise control of film thickness, roughness, homogeneity, and crystal orientation by the solute concentration and growth environment, thereby enabling further studies to achieve orientation-controlled polarization and customizable ferroelectric properties for memory elements and sensors.

[1]Department of Mechanical Engineering and Temple Materials Institute, Temple University, Philadelphia, PA 19122, USA. [2]Ordered Matter Science Research Center, Southeast University, Nanjing 211189, P. R. China. [3]Department of Chemistry, Temple University, Philadelphia, PA 19122, USA. [4]Department of Materials Science and Engineering, University of Maryland, College Park, MD 20742, USA. *Corresponding author. Email: wuttig@umd.edu (M.W.); xiongrg@seu.edu.cn (R.-G.X.); shenqiang.ren@temple.edu (S.R.)

RESULTS

We applied this novel IP-LP thin-film growth principle to imidazolium perchlorate ($ImClO_4$) (*9*, *16*). In this case, the surface tension and high spreading ability combine to crystallize the MOFE $ImClO_4$ thin film on the surface of the solution, stabilized by the hydrogen bonding between water and imidazolium molecules. The supersaturated $ImClO_4$ aqueous solution is kept at 363 K in a controlled water vapor environment to tune the evaporation rate or external water partial pressure. At the surface of supersaturated $ImClO_4$ solution, layer-like nucleation occurs, which mimics the upper dipole layer of $ImClO_4$ and thereby permits in-plane "epitaxial" growth of this material (Fig. 1A). The controlled evaporation and thermal gradient between the surface and $ImClO_4$ solution drive solute Marangoni flow (*23*, *24*), resulting in lateral epitaxial growth of the MOFE $ImClO_4$ film on the liquid surface. Simultaneous rapid evaporation leads to higher supersaturation and therefore fast growth of the transparent $ImClO_4$ film (Fig. 1B). Figure 1B displays how the rapid growth yields a bamboo-like continuous film with an average thickness of d = 390 nm. The $ImClO_4$ film morphology shown in Fig. 1B is created by the depolarization field of the MOFE as the film is synthesized below the Curie temperature. Hence, the $ImClO_4$ nuclei will coalesce into the equilibrium "twin" structure, which represents a compromise between the intervariant interface and depolarization energy densities (Fig. 1, C and D) (*25*). Figure S7 shows the x-ray diffraction patterns of the as-grown $ImClO_4$ film and indium tin oxide (ITO) substrate together with their simulations. After subtracting the ITO peaks, the remaining peaks are assigned to a hexagonal $ImClO_4$ lattice with $a = b$ = 8.11 Å. The two distinct peaks located at 21.89° and 24.27° suggest that the as-prepared transparent $ImClO_4$ film is composed of highly oriented $(2,\bar{1},0)$ and $(1,0,\bar{2})$ variants. Pawley refinement returned more precise hexagonal cell dimensions of $a = b$ = 8.1079 Å, corresponding to the noncentrosymmetric trigonal space group *R*3*m* (insets in Fig. 1A and fig. S8) (*26*). The thickness of an $ImClO_4$ film can be tuned by the evaporation rate of the water or external water partial pressure. An external water vapor flow of different saturated external water partial pressure has been used to modify the water partial pressure above the supersaturated solution to control the growth rate and the uniformity of $ImClO_4$ crystalline films (Fig. 1E). Higher external water partial pressure via vapor flow, which is between 10.2% at

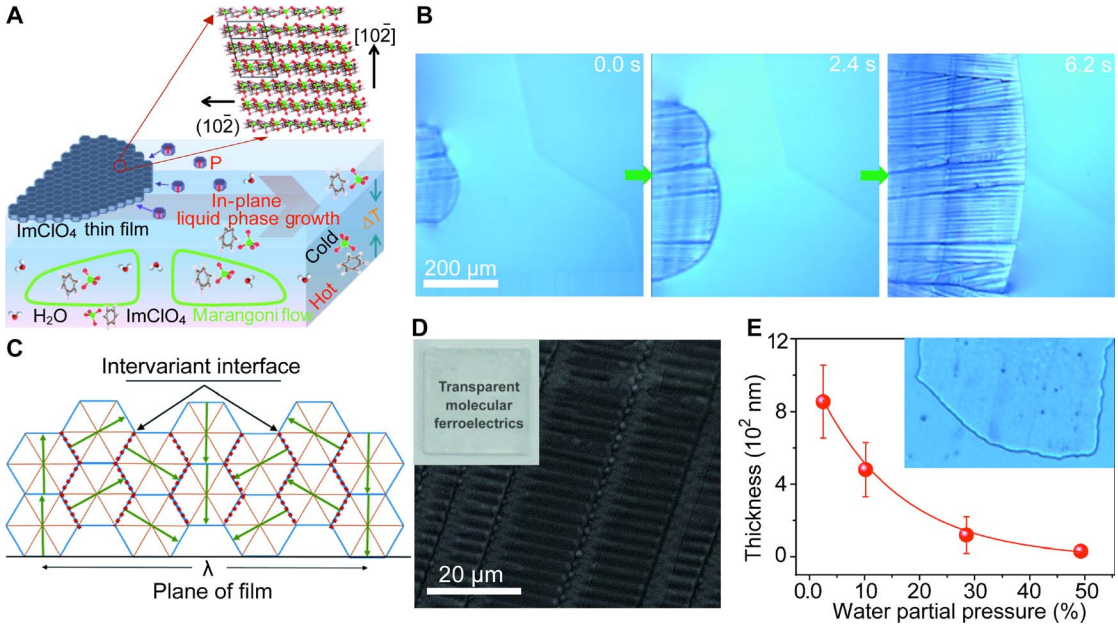

Fig. 1. Schematic illustration of the formation process of a MOFE $ImClO_4$ thin film and its corresponding morphology. (**A**) IP-LP growth by controlled supersaturation at the liquid-air interface with controlled temperature gradient and external water partial pressure. (**B**) Typical growth process of an $ImClO_4$ thin film with an average thickness of 390 nm, recorded by an optical microscope on the gas/water surface at a low external water partial pressure. (**C**) Schematic figure of the "twin-like" grown MOFE $ImClO_4$ films with *n* intervariant interfaces. The sum of the intervariant interface and depolarization energies, $n\gamma A$ and $\varepsilon_r P_s^2 V$, admits to a minimum at the wavelength $\lambda = (\frac{\gamma t}{\varepsilon_r p_s^2})^{1/2}$, where $V/A = t$ is the film thickness. (**D**) Scanning electron microscopy image of the $ImClO_4$ thin film with a bamboo-like surface morphology with an average thickness of 390 nm. The inset displays the as-grown transparent $ImClO_4$ film. (**E**) External water partial pressure–dependent thickness control of the $ImClO_4$ thin film. The partial water pressure above the supersaturated $ImClO_4$ solution was used to control the growth rate and the uniformity of the $ImClO_4$ crystallized film.

328 K and 58.1% at 363 K here, decreases the evaporation rate of the water at the surface of the solution. The supersaturation gradient that evolves at the surface of the solution leads to the formation of nuclei at the surface. Good crystallinity is achieved by slowing the growth rate of the $ImClO_4$ film through controlling the external water vapor flow.

The ferroelectricity of $ImClO_4$ thin films is demonstrated by the polarization–electric field hysteresis loop (Fig. 2A). It can be attributed to the small permanent dipole moment of the slightly distorted ClO_4^- anion together with the contribution from the off-center displacement of the Im^+ cation (fig. S7) (*16*) and switched at kilohertz frequencies. The measured spontaneous saturation polarization of $ImClO_4$ thin films is as high as 6.7 μC/cm^2, compared to the values 1 μC/cm^2 for irregularly structured bulk material (*27*) and 23 μC/cm^2 for inorganic perovskite $BaTiO_3$ (*28*). The coercive field of 5 kV/cm equals $^1/_{10}$ of that of perovskite oxide ferroelectrics (*29*), making it an ideal candidate for molecular electronics with low-energy consumption. Piezoresponse force microscopy (PFM) (Fig. 2, B to D) confirms the ferroelectric properties of the as-grown $ImClO_4$ thin films. The domain boundaries, the yellow/purple-colored region, represent 180° subboundaries. We monitored polarization switching of the MOFE $ImClO_4$ films through their electromechanical response using PFM at a fixed tip position on the film surface as a function of a cyclic writing voltage, revealing a clear hysteresis and butterfly behavior (Fig. 2E). The distinct 180° domain switching in precise 180° intervals further corroborates a robust ferroelectric polarization in $ImClO_4$ thin films. Notably, the phase of the PFM response signal corresponds directly to the direction of the electric polarization of the microscopic region of the surface monitored under the tip. Thus, the hysteretic switching of the response signal phase by 180° in response to a sweeping dc voltage is attributed to the electric switching of polarization according to the direction of the electric field (Fig. 2E, top). The hysteretic 180° phase switching observed in the PFM response represents evidence of local ferroelectricity of the $ImClO_4$ films. The amplitude signal obtained from the PFM image (Fig. 2E, bottom) is directly correlated to the local strain of the $ImClO_4$ film experienced by the cantilever. Together, the hysteretic amplitude and the butterfly loops confirm the piezoelectricity of $ImClO_4$ films.

Our observation allows us to determine the piezoelectric voltage and piezoelectric strain constants, $g = d/\varepsilon_0\varepsilon_r$ and $x = d{\cdot}E$, where d is the piezoelectric charge constant and ε_0 and ε_r are the vacuum dielectric constant and the relative dielectric constant, respectively (*30*–*34*). To demonstrate the electromechanical coupling of a piezoelectric $ImClO_4$ film, we sandwiched the film between two electrodes and applied a periodic mechanical stress using a dynamic mechanical test system. The generated electrical output signal was recorded by measuring the current and voltage outputs. Figure 2 (F and G) shows the piezoelectric current and voltage responses of the $ImClO_4$ thin films. The signals reverse polarity, corresponding to the alternating compression and tension along the $[1,0,\bar{2}]$ direction. Typical peak current and voltage values are 3.2 nA and 0.073 V, respectively. The time-integrated single current peak yields a charge, $Q \approx 3.8 \times 10^2$ pC, generated at an applied peak load of $F = 9.8$ N. We can thus estimate the global piezoelectric coefficient $d_{33} = Q/F = 38.8$ pm/V, which is similar to the local value measured by PFM in $ImClO_4$ thin films. The piezoelectric coefficient measured by the polarity switching from PFM measurement and force-induced current/voltage signal confirms that the electrical signals stem from the piezoelectric $ImClO_4$ thin films. Figure 2 (H and I) and figs. S8 to S11 further demonstrate that the piezoelectric signal is linear in a range of 0.73 to 3.2 nA or 0.013 to 0.068 V. The electromechanical energy conversion is reversible and repeatable in more than 1000 cycles (Fig. 2I, inset), as required for devices.

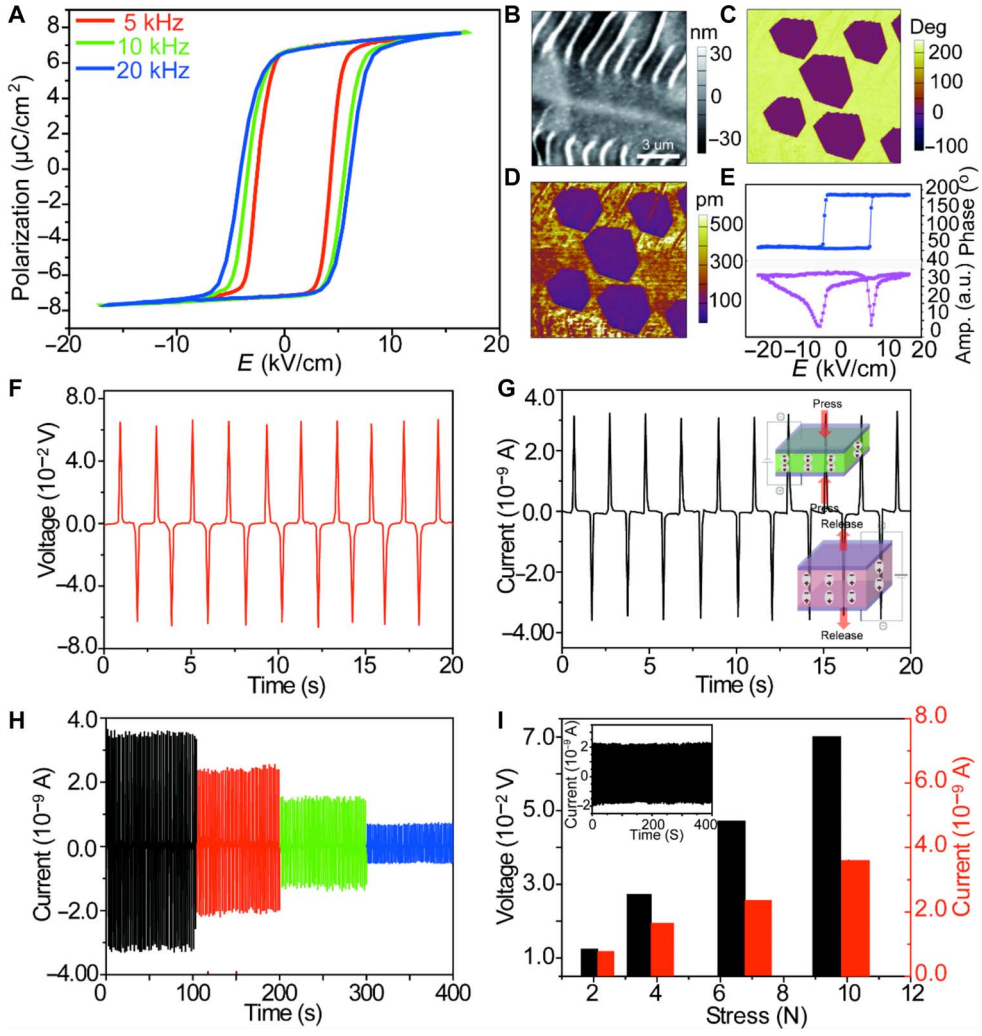

Fig. 2. Electromechanical coupling in $ImClO_4$ thin films. (**A**) Ferroelectric hysteresis loop of an $ImClO_4$ film. (**B** to **D**) Atomic force microscopy (AFM) height images and corresponding PFM phase and amplitude patterns of $ImClO_4$ film. (**E**) Local PFM hysteresis loops of $ImClO_4$ film. Top: Phase signal. Bottom: Amplitude signal. a.u., arbitrary units. (**F** and **G**) Piezoelectric current and voltage responses on an $ImClO_4$ thin film at an external force of 9.8 N. The polarity reverses upon applying and releasing the force. The inset displays a schematic illustration of the piezoelectric effect of ferroelectric $ImClO_4$ thin films. (H and I) Stress (σ), induced output current (*I*), and voltage (*V*) in the range of 2.4 N ≤ σ ≤ 9.8 N, leading to the enhanced current 0.73 nA ≤ *I* ≤ 3.2 nA and voltage 0.013 V ≤ *V* ≤ 0.068 V. The output current exhibits excellent reversibility and repeatability for the cyclic loading of 7.8 N for 500 cycles, as illustrated by the inset of (I).

A unique feature of transparent MOFE $ImClO_4$ thin films is the large electro-optic activity (*35*, *36*), which we characterized through polarization light spectroscopy. We use a broadband polarization rotator to control the polarization direction of a beam of 488-nm laser light incident on an $ImClO_4$ film and record the resultant luminescence images from the film (Fig. 3A). The polarization-dependent luminescence is depicted in Fig. 3B. As the angle of the polarizer rotates, the intensity increases to a maximum at 0°/180° and decreases to a minimum at 90°/270° when the electric field vector of incident light, $\vec{E}$, is parallel or antiparallel to the vector of polarization, $\vec{P}$. The linearly polarized light of wave vector $\vec{k}$, interacting with the polarization $P_{2\bar{1}0}$, can lead to a strong light-matter interaction because of the linear electro-optic effect of transparent ferroelectric $ImClO_4$ films. The electric field–dependent transmittance of the transparent $ImClO_4$ films can also be used to investigate domain inversion or polarization switching. We find that our $ImClO_4$ films show a strong and repeatable contrast change under cyclic poling (Fig. 3, C and D). Studies of the transmission spectrum of $ImClO_4$ films from 450 to 1000 nm revealed strong contrast changes in the poled areas. Figure 3D represents a comparison of transmission spectra between three different domain states during a poling cycle: original and negatively and positively poled states. Negative saturation poling decreases the transmission with a modulation of 3%, as obtained from the integral area of transmission spectrum (350 to 1100 nm). Positive saturation poling reverts to the unmodulated state. The transmittance of $ImClO_4$ films can thus be varied by the linear electro-optic, piezoelectric, and interference effects. In an electro-optic material, such as MOFE $ImClO_4$, the refractive index increases to $n + \Delta n$ under positive poling, whereas it decreases to $n - \Delta n$ under negative poling. The linear electro-optical effect induced the modulation of the refractive index, $\Delta n \propto \varepsilon \cdot E$, where ε is the electro-optic tensor. The index difference, Δn, results from the phase retardation of the transmitted beam in the $ImClO_4$ films. A second phase retardation due to the piezoelectric effect is caused by the thickness variation, $\pm\Delta d$, in the reversed domain. During poling, an incident plane wave experiences a phase shift $\Delta\varphi$,

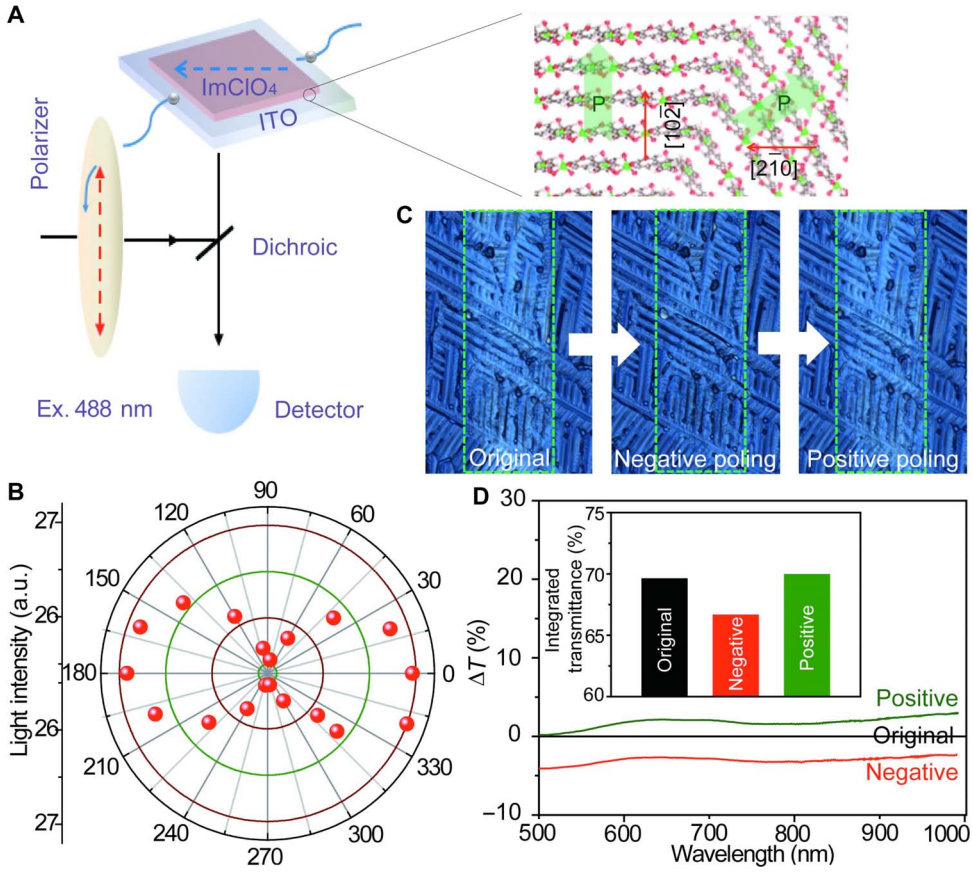

Fig. 3. Electro-optic effect of $ImClO_4$ thin films. (**A**) Diagram of the apparatus used to determine the angle-dependent polarization. The light-matter interaction is strongest when the polarization vectors of the $ImClO_4$ thin film are directed parallel to the [2,$\bar{1}$,0] direction. (**B**) Angle-dependent transmitted light intensity of $ImClO_4$ thin film. (**C**) Optical images of negatively and positively poled $ImClO_4$ thin films. Green rectangles represent the electrode area. (**D**) Comparison of the transmission spectra of the original and negatively and positively poled states. The inset shows the transmittance of the $ImClO_4$ thin film on ITO substrate at three different states.

because of the linear electro-optic and piezoelectric effects, which, along the [2,$\bar{1}$,0] axis, is given by (*37*)

$$\Delta\phi = 2\left[\frac{2\pi}{\lambda}\Delta n d + \frac{2\pi}{\lambda}(n_0 - n_w)\Delta d)\right] = [-\varepsilon n_0^3 + 2(n_0 - n_w)k_3]V$$

where V is the poling voltage, n_0 is the refractive index, Δn is the refractive index change, λ is the wavelength of light, and Δd is the piezoelectric thickness change dependent on the constant k_3 (the ratio between the linear piezoelectric and the stiffness tensor $n_w = 1.33$). The equation illustrates how the thin-film interference pattern of MOFE $ImClO_4$ is determined by the piezoelectric and electro-optic characteristics (*38*–*40*).

MOFE thin films that are electrically switchable at room temperature can facilitate organic electronic memory elements (*41*–*43*). As shown in Fig. 4A, conducting AFM and related PFM images performed on $ImClO_4$ films reveal a distinct local resistance contrast between the upward and downward polarization domains. When an electric poling field (writing voltage) is applied on the $ImClO_4$ film, the polarization is directed parallel to the electric field direction, and the potential barrier encountered by the electrons is reduced, leading to an increased circuit current and a reduced electroresistance, termed ON state (Fig. 4B, left). When the electric field is switched, the dipole direction is reversed, and the increased average height of the potential barrier leads to a reduced current and an increased electroresistance, termed OFF state (Fig. 4B, right). Therefore, we applied a positive/reverse writing field larger than the coercivity to polarize the dipoles in the same direction. Simultaneously, we applied a reading field smaller than the coercivity to investigate the resistive switching of MOFE $ImClO_4$ thin films. Figure 4C shows the continuous, nonlinear, and symmetric current-voltage (*I*-*V*) curves for the ON and OFF states, with a small reading field corresponding to a voltage between −0.5 and 0.5 V. The pronounced 2400% difference of the *I*-*V* curves indicates the electroresistance of the $ImClO_4$ film. The current ratio of the ON and the OFF states (Fig. 4D) further confirms the polarization-modulated electroresistance of the $ImClO_4$ film, in which an average OFF/ON ratio of about 20 has been achieved. Figure 4E presents the retention performance of MOFE $ImClO_4$ thin films at V_{read} = 0.2 V for the ON and OFF states, which exhibit resistances of 1.5×10^7 and 7.2×10^6 ohms, respectively. There is no significant deterioration both in the ON and OFF states, indicating good information retention of $ImClO_4$ thin films. The inset of Fig. 4E shows near-identical *I*-*V* curves before and after a 5-hour retention time in both ON and OFF states, suggesting very small switching fatigue of the $ImClO_4$ films. The switching performance of $ImClO_4$ films is further tested by repeatedly switching the ferroelectric barrier with positive and reverse poling (writing). Again, polarization switching–induced electroresistance with good reproducibility is achieved and shown in

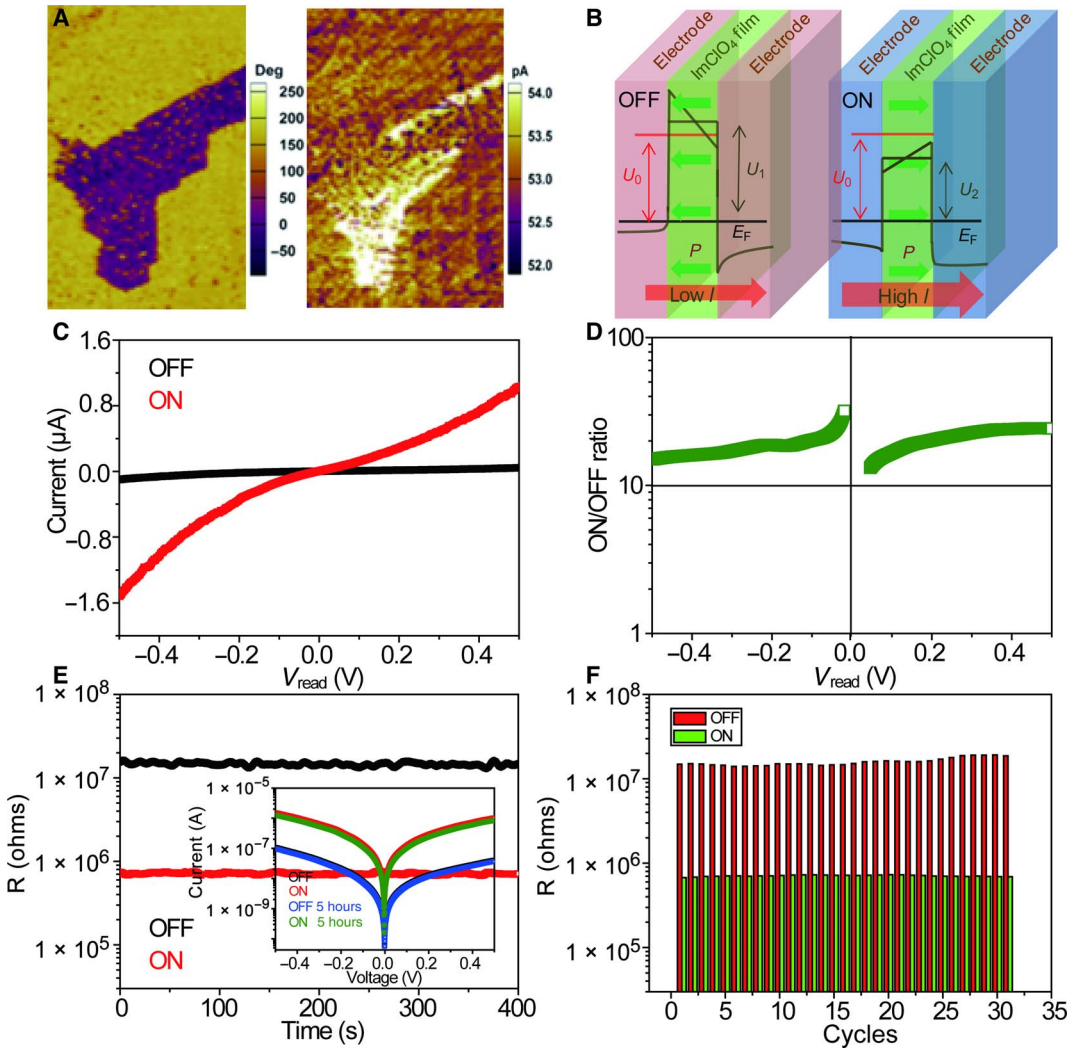

Fig. 4. Polarization-induced resistance switching of MOFE $ImClO_4$ thin films. (**A**) Conducting AFM and related PFM images reveal a distinct resistance contrast between the upward and downward polarized domains. (**B**) Schematic illustration of the polarization switching–induced resistance of MOFE $ImClO_4$ thin films. When the film polarization is directed parallel to the electric field, the potential barrier of the electrons is reduced (ON state), whereas the average height of the potential barrier increases when the direction of the polarization is reversed (OFF state), resulting in an increase and/or decrease of the resistance. (**C**) *I-V* curves in the ON and OFF states for a small reading voltage between −0.5 and 0.5 V. (**D**) Current ratio between the ON and OFF states of $ImClO_4$ thin-film devices. (**E**) Device retention performance at V_{read} = 0.2 V for the ON and OFF states; no significant deterioration was found in both the ON and OFF resistance levels after cycling 10^3 times. The inset shows the *I-V* curves before and those of both the ON and OFF states after 10^3 cycles. (**F**) Cyclic polarization switching tests the ON and OFF resistance stability of $ImClO_4$ thin-film devices.

Fig. 4F. The ON/OFF resistance ratio of about 20 is maintained in more than 30 write/read cycles. Future nonvolatile resistive memory elements based on molecular $ImClO_4$ films with high electroresistance and fatigue resistance comparable to ferroelectric polymers thus appear possible.

DISCUSSION

In summary, we show in this study that films of the MOFE $ImClO_4$ have all the characteristics desirable in a candidate material for nanoelectronic devices. Films of $ImClO_4$, fabricated using a novel technique—controlled supersaturation growth at the liquid-air interface under temperature gradient and external water partial pressure—are transparent and consist of a bamboo-like structure of $(2,\bar{1},0)$ and $(1,0,\bar{2})$ variants of *R*3*m* symmetry. The $ImClO_4$ thin films show the Curie temperature of 373.6 K and a room temperature reversibly switchable polarization of 6.7 μC/cm^2, as well as a reversible electromechanical response, d_{33} = 38.8 pm/V. Polarization switching results in a 30% change of the refractive index of single domains. Foremost, the electroresistance of the films changes reversibly by a factor of 20 upon polarization switching without fatigue. The $ImClO_4$ MOFE thin film that we describe here thus represents an attractive multifunctional material that will germinate a new generation of molecular electronic sensing, actuation, data, and energy storage devices.

MATERIALS AND METHODS

Synthesis of $ImClO_4$ molecular film by an IP-LP growth with controlled water evaporation rate

A near-supersaturated $ImClO_4$ solution (~700 mg/ml at 363 K) on an ITO-patterned glass substrate was used to synthesize the $ImClO_4$ thin films. We started the synthesis by transferring supersaturated $ImClO_4$

solution onto the substrate preheated at 363 K. The higher supersaturation at the surface leads to surface nucleation of the $ImClO_4$ film. Because of the high surface tension and high spreading ability, the film nucleus floats on the solution surface, stabilized by the hydrogen bonding between water and imidazolium molecules. The evaporation-induced lower temperature of the surface creates a thermal gradient between the surface and the bottom of the solution, resulting in Marangoni flow of $[IM]^+$ and $[ClO_4]^-$ from the bottom to the surface, leading to IP-LP epitaxy of the film on the surface of the solution.

An external water vapor flow with a different water partial pressure, controlled by nitrogen gas from a second heated water container, kept at a different temperature was used to set an artificial nonequilibrium partial pressure of water above the solution, thereby controlling the growth rate and uniformity of the $ImClO_4$ crystallized film. The partial pressure of water, ranging from 10.2% at 328 K to 58.1% at 363 K, was monitored with a pressure sensor. This arrangement maintained a steady-state film growth of controllable thickness and quality. In general, higher growth rates promoted thicker films, whereas lower growth rates induced a lower surface roughness. After removing the bottom solution by super absorptive materials, the smooth film can be readily transferred to a device, which was further vacuum-treated for more than 2 hours before subsequent use. For this study, we adopted large-area continuous films synthesized by rapid growth.

Morphology and structure characteristics

Real-time measurements of optical images were recorded by an Olympus BX51 microscope and were computer-processed. Scanning electron microscopy images were taken via FEI Quanta 450 FEG. X-ray diffraction analysis was carried out using a Rigaku charge-coupled device diffractometer with Mo-Kα radiation (λ = 0.71073 Å). Data collection, cell refinement, and data reduction were performed using Rigaku CrystalClear software. The crystal structures were refined by the full-matrix method using the SHELXL97 software package.

Characteristics of ferroelectric properties

Room temperature polarization hysteresis loops were obtained by Radiant Precision Premier LC II, in air at measurement frequencies of 5, 10, and 20 kHz. PFM was conducted using Asylum Research MFP-3D and Bruker Multimode 8 atomic force microscopes equipped with a conductive cantilever having a spring constant of 2 N/m. The PFM mappings were obtained with a 400-mV ac voltage excitation. A dc voltage was superimposed to switch the polarization. The square wave output, 2 V and 41 kHz, of a conductive AFM tip (MESP-RC, Co/Cr coating, 35-nm tip radius) was used to observe phase and amplitude variations.

Fabrication of resistance switching devices

We prepared ITO/$ImClO_4$/100-nm Ag sandwiches to determine the resistance of the $ImClO_4$ films. The ~400-nm $ImClO_4$ film was transferred onto the ITO-prepatterned glass substrate and annealed in a vacuum oven for 2 hours, and then a 100-nm Ag film was deposited onto the molecular film through a shadow mask to serve as the top electrode. The dimension of the electrically active area was 0.1 cm × 0.1 cm. All sandwiches were characterized in a darkened glove box. An external voltage of 2 V from an Agilent 8114A 001 pulse generator, producing a field of 50 kV/cm, was applied to the electrodes to determine resistance switching characteristics using a Keithley 4200A-SCS multimeter.

Fabrication of piezoelectric and pyroelectric devices

After the $ImClO_4$ film was transferred onto the ITO-patterned glass substrate and dried in vacuum, a 100-nm silver film was deposited on top of the film through a shadow mask to serve as the top electrode. After soldering signal wires to the silver electrodes, the assembly was sealed in a 4-mm-thick polydimethylsiloxane (PDMS) matrix to assure structural stability for the piezoelectric tests. All devices used in this study were poled by an applied voltage of 5 V. The piezoelectric device was driven by a dynamic mechanical test system (ElectroForce 3200, Bose). A Keithley 4200A-SCS instrument recorded the current and open circuit voltage characteristics as a function of the varying stress. The impedance used to measure voltage is 1 megohm. A thermoelectric element was used to change the temperature of the device, monitored by a sensor on top of the device. The voltage and current outputs were recorded as for the piezoelectric measurements. All devices were characterized in a glove box.

Optical measurement

For the angle-dependent fluorescence measurement, a thin film was mounted on an Olympus IX73 inverted microscope. Fluorescence was excited with a 488-nm laser and collected with a Princeton Instruments ACTON SpectraPro 2500i/Spec-10 spectrometer using a 20× objective. A linear polarizer in the detection path served to select defined polarization vectors. Pulses of ±2 V were applied to the device from an Agilent 8114A 001 pulse generator to switch the polarization. The optical contrast images before and after poling of molecular films were captured by an Olympus BX51 microscope. The transmission spectra of different polarization states were determined by a spectrometer that detected the variations of the collimated light over the entire electrode.

Note that the Im molecule and the perchlorate ion may both cause irriration to eyes and skin. Therefore, it is better to wear fitting goggles, protective gloves, and clothes when performing the experiments.

SUPPLEMENTARY MATERIALS

Supplementary material for this article is available at http://advances.sciencemag.org/cgi/content/full/3/8/e1701008/DC1

fig. S1. Optical images of $ImClO_4$ molecular crystals synthesized by spin coating an $ImClO_4$ solution (700 mg/ml) on an ITO-prepatterned glass substrate at 3000 rpm, at different magnifications.

fig. S2. Optical images of $ImClO_4$ molecular crystals synthesized by drop-casting $ImClO_4$ solution on ITO glass substrate at a concentration of 700 mg/ml, at different magnifications.

fig. S3. Optical images of $ImClO_4$ molecular films synthesized by IP-LP growth on ITO glass substrate at an intermediate evaporation rate, with a water partial pressure of 13.5%; the film grows on the surface of the solution, inducing unidirectional growth.

fig. S4. Optical images of $ImClO_4$ molecular films synthesized by IP-LP growth on ITO glass substrate at a slow evaporation rate, with a water partial pressure of 45.1%, at different magnifications.

fig. S5. Morphology and elements distribution analysis of $ImClO_4$ molecular films at a water partial pressure of 45.1%.

fig. S6. Morphology and elements distribution analysis of $ImClO_4$ molecular films at a water partial pressure of 35.5%.

fig. S7. Experimental and simulated x-ray diffraction patterns of $ImClO_4$ film on ITO substrate.

fig. S8. Piezoelectric voltage response of the Ag/$ImClO_4$/Ag sandwiches to external stresses from 2.4, 4.1, and 6.7 to 9.8N, which generate the proportional voltages shown in the right-hand side.

fig. S9. Evolution of the piezoelectric current outputs at different applied stresses from 2.4, 4.1, and 6.7 to 9.8 N on the $ImClO_4$ film.

fig. S10. Evolution of the piezoelectric voltage outputs with decreasing magnitude of the applied stress on the $ImClO_4$ film from 2.4, 4.1, and 6.7 to 9.8 N.

fig. S11. Piezoelectric voltage as a function of the frequency resulting from applied forces, $F_0\sin(vt)$ (F_0 = 4.5 N at 0.40, 0.20, and 0.10 Hz).

REFERENCES AND NOTES

1. J. Valasek, Piezo-electric and allied phenomena in Rochelle salt. *Phys. Rev.* **17**, 475 (1921).
2. S. Horiuchi, Y. Tokura, Organic ferroelectrics. *Nat. Mater.* **7**, 357–366 (2008).
3. D.-W. Fu, H.-L. Cai, Y. Liu, Q. Ye, W. Zhang, Y. Zhang, X.-Y. Chen, G. Giovannetti, M. Capone, J. Li, R.-G. Xiong, Diisopropylammonium bromide is a high-temperature molecular ferroelectric crystal. *Science* **339**, 425–428 (2013).

4. A. S. Tayi, A. K. Shveyd, A. C.-H. Sue, J. M. Szarko, B. S. Rolczynski, D. Cao, T. J. Kennedy, A. A. Sarjeant, C. L. Stern, W. F. Paxton, W. Wu, S. K. Dey, A. C. Fahrenbach, J. R. Guest, H. Mohseni, L. X. Chen, K. L. Wang, J. F. Stoddart, S. I. Stupp, Room-temperature ferroelectricity in supramolecular networks of charge-transfer complexes. *Nature* **488**, 485–489 (2012).
5. H.-Y. Ye, J.-Z. Ge, Y.-Y. Tang, P.-F. Li, Y. Zhang, Y.-M. You, R.-G. Xiong, Molecular ferroelectric with most equivalent polarization directions induced by the plastic phase transition. *J. Am. Chem. Soc.* **138**, 13175–13178 (2016).
6. K. Asadi, D. M. de Leeuw, B. de Boer, P. W. M. Blom, Organic non-volatile memories from ferroelectric phase-separated blends. *Nat. Mater.* **7**, 547–550 (2008).
7. R. C. G. Naber, K. Asadi, P. W. M. Blom, D. M. de Leeuw, B. de Boer, Organic nonvolatile memory devices based on ferroelectricity. *Adv. Mater.* **22**, 933–945 (2010).
8. Q. Ye, Y.-M. Song, G.-X. Wang, K. Chen, D.-W. Fu, P. W. H. Chan, J.-S. Zhu, S. D. Huang, R.-G. Xiong, Ferroelectric metal–organic framework with a high dielectric constant. *J. Am. Chem. Soc.* **128**, 6554–6555 (2006).
9. W. Gao, L. Chang, H. Ma, L. You, J. Yin, J. Liu, Z. Liu, J. Wang, G. Yuan, Flexible organic ferroelectric films with a large piezoelectric response. *NPG Asia Mater.* **7**, e189 (2015).
10. S. Hoshino, T. Mitsui, F. Jona, R. Pepinsky, Dielectric and thermal study of tri-glycine sulfate and tri-glycine fluoberyllate. *Phys. Rev.* **107**, 1255 (1957).
11. H. S. Nalwa, S. Miyata, *Nonlinear Optics of Organic Molecules and Polymers* (CRC Press, 1996).
12. M. Pandeeswar, S. P. Senanayak, K. S. Narayan, T. Govindaraju, Multi-stimuli-responsive charge-transfer hydrogel for room-temperature organic ferroelectric thin-film devices. *J. Am. Chem. Soc.* **138**, 8259–8268 (2016).
13. Y. Xu, *Ferroelectric Materials and Their Applications* (Elsevier, 1991).
14. J. M. Herbert, *Ferroelectric Transducers and Sensors* (CRC Press, 1982), vol. 3.
15. S. Horiuchi, Y. Tokunaga, G. Giovannetti, S. Picozzi, H. Itoh, R. Shimano, R. Kumai, Y. Tokura, Above-room-temperature ferroelectricity in a single-component molecular crystal. *Nature* **463**, 789–792 (2010).
16. Y. Zhang, Y. Liu, H.-Y. Ye, D.-W. Fu, W. Gao, H. Ma, Z. Liu, Y. Liu, W. Zhang, J. Li, G.-L. Yuan, R.-G. Xiong, A molecular ferroelectric thin film of imidazolium perchlorate that shows superior electromechanical coupling. *Angew. Chem. Int. Ed.* **53**, 5064–5068 (2014).
17. H.-Y. Ye, Q. Zhou, X. Niu, W.-Q. Liao, D.-W. Fu, Y. Zhang, Y.-M. You, J. Wang, Z.-N. Chen, R.-G. Xiong, High-temperature ferroelectricity and photoluminescence in a hybrid organic–inorganic compound: (3-Pyrrolinium)$MnCl_3$. *J. Am. Chem. Soc.* **137**, 13148–13154 (2015).
18. X.-L. Li, K. Chen, Y. Liu, Z.-X. Wang, T.-W. Wang, J.-L. Zuo, Y.-Z. Li, Y. Wang, J. S. Zhu, J.-M. Liu, Y. Song, X.-Z. You, Molecule-based ferroelectric thin films: Mononuclear lanthanide enantiomers displaying room-temperature ferroelectric and dielectric properties. *Angew. Chem. Int. Ed.* **46**, 6820–6823 (2007).
19. J.-P. Yang, Q. Liao, J.-J. Zhou, X. Jiang, X.-H. Wang, Y. Zhang, S.-D. Jiang, S.-K. Yan, L. Li, What determines the lamellar orientation on substrates? *Macromololecules* **44**, 3511–3516 (2011).
20. L. Gránásy, T. Pusztai, T. Börzsönyi, J. A. Warren, J. F. Douglas, A general mechanism of polycrystalline growth. *Nat. Mater.* **3**, 645–650 (2004).
21. D. Damjanovic, Ferroelectric, dielectric and piezoelectric properties of ferroelectric thin films and ceramics. *Rep. Prog. Phys.* **61**, 1267 (1998).
22. R. E. Eitel, C. A. Randall, T. R. Shrout, S.-E. Park, Preparation and characterization of high temperature perovskite ferroelectrics in the solid-solution (1-*x*) $BiScO_3$–*x*$PbTiO_3$. *Jpn. J. Appl. Phys.* **41**, 2099 (2002).
23. E. Hendarto, Y. B. Gianchandani, Size sorting of floating spheres based on Marangoni forces in evaporating droplets. *J. Micromech. Microeng.* **23**, 075016 (2013).
24. P. Lovass, M. Branicki, R. Tóth, A. Braun, K. Suzuno, D. Ueyama, I. Lagzi, Maze solving using temperature-induced Marangoni flow. *RSC Adv.* **5**, 48563–48568 (2015).
25. A. G. Khachaturyan, *Theory of Structural Phase Transformations in Solids* (John Willey, 1983), pp. 1733–1743.
26. G. S. Pawley, Unit-cell refinement from powder diffraction scans. *J. Appl. Crystallogr.* **14**, 357–361 (1981).
27. Z. Pająk, P. Czarnecki, B. Szafrańska, H. Małuszyńska, Z. Fojud, Ferroelectric ordering in imidazolium perchlorate. *J. Chem. Phys.* **124**, 144502 (2006).
28. Z. Cui, K. Gao, C. Liu, Y. Yin, D.-W. Fu, H.-L. Cai, X. S. Wu, Molecular ferroelectric pyridin-4-ylmethanaminium perchlorate undergoes paraelectric–ferroelectric and ferroelectric–ferroelectric phase transitions. *J. Phys. Chem. C* **120**, 2925–2931 (2016).
29. J. Wang, J. B. Neaton, H. Zheng, V. Nagarajan, S. B. Ogale, B. Liu, D. Viehland, V. Vaithyanathan, D. G. Schlom, U. V. Waghmare, N. A. Spaldin, K. M. Rabe, M. Wuttig, R. Ramesh, Epitaxial $BiFeO_3$ multiferroic thin film heterostructures. *Science* **299**, 1719–1722 (2003).
30. S. R. Anton, H. A. Sodano, A review of power harvesting using piezoelectric materials (2003–2006). *Smart Mater. Struct.* **16**, R1 (2007).
31. S.-E. Park, T. R. Shrout, Ultrahigh strain and piezoelectric behavior in relaxor based ferroelectric single crystals. *J. Appl. Phys.* **82**, 1804 (1997).
32. C. R. Bowen, H. A. Kim, P. M. Weaver, S. Dunn, Piezoelectric and ferroelectric materials and structures for energy harvesting applications. *Energy Environ. Sci.* **7**, 25–44 (2014).
33. J. Li, Y. Liu, Y. Zhang, H.-L. Cai, R.-G. Xiong, Molecular ferroelectrics: Where electronics meet biology. *Phys. Chem. Chem. Phys.* **15**, 20786–20796 (2013).
34. S. Xu, Y. Qin, C. Xu, Y. Wei, R. Yang, Z. L. Wang, Self-powered nanowire devices. *Nat. Nanotechnol.* **5**, 366–373 (2010).
35. F. Jona, G. Shirane, *Ferroelectric Crystals* (Pergamon, 1962), vol. 1.
36. H.-S. Kitzerow, H. Molsen, G. Heppke, Linear electro-optic effects in polymer-dispersed ferroelectric liquid crystals. *Appl. Phys. Lett.* **60**, 3093–3095 (1992).
37. S. Grilli, P. Ferraro, M. Paturzo, D. Alfieri, P. De Natale, M. de Angelis, S. De Nicola, A. Finizio, G. Pierattini, In-situ visualization, monitoring and analysis of electric field domain reversal process in ferroelectric crystals by digital holography. *Opt. Express* **12**, 1832–1842 (2004).
38. V. Gopalan, T. E. Mitchell, In situ video observation of 180° domain switching in $LiTaO_3$ by electro-optic imaging microscopy. *J. Appl. Phys.* **85**, 2304–2311 (1999).
39. J. Yao, X. Zhao, X.-Q. Yan, C. Gao, X.-D. Chen, W. Xin, Y. Chen, Z.-B. Liu, J.-G. Tian, Polarization dependence of optical pump-induced change of graphene extinction coefficient. *Opt. Mater. Express* **5**, 1550–1559 (2015).
40. V. Gopalan, Q. X. Jia, T. E. Mitchell, In situ video observation of 180° domain kinetics in congruent $LiNbO_3$ crystals. *Appl. Phys. Lett.* **75**, 2482 (1999).
41. S. J. Kang, Y. J. Park, I. Bae, K. J. Kim, H.-C. Kim, S. Bauer, E. L. Thomas, C. Park, Printable ferroelectric PVDF/PMMA blend films with ultralow roughness for low voltage non-volatile polymer memory. *Adv. Funct. Mater.* **19**, 2812–2818 (2009).
42. J. F. Scott, C. A. Paz de Araujo, Ferroelectric memories. *Science* **246**, 1400–1405 (1989).
43. J. F. Scott, *Ferroelectric Memories* (Springer Science and Business Media, 2013), vol. 3.

Acknowledgments

Funding: Work at the Temple University (S.R.) supported by the U.S. Department of Energy, Office of Basic Energy Sciences, Division of Materials Sciences and Engineering, under Award DE-SC0017928. Work at the Temple University (A.J.W. and K.W.) was supported by the Department of Energy, Office of Science, Basic Energy Science under award #DE-SC0010307. Work at the Southeast University was supported by the National Natural Science Foundation of China (NSFC-91622104 and NSFC-21427801). Work at the University of Maryland, College Park (M.W.) was supported by the Army Research Office contract W911NF-15-1-0615.
Author contributions: Z.Z. carried out experiments and wrote the paper. P.-F.L. and Y.-Y.T. performed the x-ray diffraction measurement and measured the ferroelectric properties. A.J.W. and K.W. designed and performed the angle-dependent optical measurement. S.R., R.-G.X., and M.W. guided the project and edited the manuscript. All authors discussed the results and commented on the manuscript. **Competing interests:** The authors declare that they have no competing interests. **Data and materials availability:** All data needed to evaluate the conclusions in the paper are present in the paper and/or the Supplementary Materials. Additional data related to this paper may be requested from the authors.

Submitted 1 April 2017
Accepted 4 August 2017
Published 30 August 2017
10.1126/sciadv.1701008

Citation: Z. Zhang, P.-F. Li, Y.-Y. Tang, A. J. Wilson, K. Willets, M. Wuttig, R.-G. Xiong, S. Ren, Tunable electroresistance and electro-optic effects of transparent molecular ferroelectrics. *Sci. Adv.* **3**, e1701008 (2017).